Modeling and Control of Bridgeless Single-Switch Non-Inverting AC-DC Cuk Converter in DCM

Humam Al-Baidhani
Department of Computer Techniques Engineering
Faculty of Information Technology
Imam Ja'afar Al-Sadiq University
Baghdad, Iraq
humam@sadiq.edu.iq

Marian K. Kazimierczuk
Department of Electrical Engineering
Wright State University
Dayton, OH 45435, USA
marian.kazimierczuk@wright.edu

Alberto Reatti
Department of Information Engineering
University of Florence
Florence 50139, Italy
alberto.reatti@unifi.it

IECON 2022 – 48th Annual Conference of the IEEE Industrial Electronics Society | 978-1-6654-8025-3/22/$31.00 ©2022 IEEE | DOI: 10.1109/IECON49645.2022.9968417

***Abstract*—In this paper, an averaged nonlinear model of a bridgeless single-switch non-inverting ac-dc Cuk converter in DCM is derived. In addition, a current-mode control scheme is designed to operate the power converter in buck and boost modes during line and load variations. In contrast, the previous research endeavors of the bridgeless Cuk converter presented a single operation mode, and accommodation of large disturbances has not been discussed. The proposed control method is compared with the classical PI controller to investigate their performance. MATLAB simulation results show that the proposed control scheme improves the dynamical response, tracks the reference voltage, and provides wide operating range.**

***Keywords*—AC-DC, bridgeless Cuk converter, current-mode control, DCM, single-switch, state-space averaged model**

I. Introduction

Switched-mode power converters play a vital role in many applications such as uninterruptible power supplies (UPS), EV chargers, and power grids [1], [2]. The power factor correction (PFC) converters are designed to provide a regulated output voltage at high efficiency and low total harmonic distortion (THD). Due to the high conduction loss in full-bridge PFC converters, the bridgeless PFC converters have been introduced to mitigate this issue [3]. For instance, the bridgeless boost converters have been proposed for ac-dc PFC applications [4], [5]. However, the boost converter is not suitable for low-voltage applications. In addition, the power converters in the previous literature contain 2 and 4 switches, which increase the control circuit complexity and conduction loss.

The ac-dc bridgeless SEPIC [6] and buck-boost [7] PFC converters have been proposed to obtain dc output voltage higher or lower than ac input voltage. Nevertheless, the multiple switches requirement has remained in the operation of these typologies. Moreover, the buck-boost operation in DCM possesses high THD due to the discontinuous input current [3], while the SEPIC typology produces high ripple at the output. Other research efforts have introduced quasi-resonant [8] and three-port quasi single-stage [9] bridgeless PFC converters, but both converters require multiple switches for operation. Totem-pole bridgeless PFC converters have also been presented to mitigate the inrush current [10] and zero-crossing distortion [11] issues. However, the complicated structure and number of required switches have been observed.

On the other hand, the ac-dc bridgeless PFC Cuk converter has been proposed in [3], [12], [13] to step the input voltage up or down. Since the output voltage of the Cuk converter is negative, an inverting amplifier is required to generate a negative feedback signal. Furthermore, the previous PFC Cuk typologies utilize dual switches for DCM operation [12], [13]. In contrast, the PFC Cuk typology in [3] requires a single switch and maintains a positive output voltage. The key advantage of the non-inverting single-switch bridgeless PFC Cuk converter is the simplicity of the control scheme as compared to the inverting multi-switch counterparts. However, the modeling of such PFC Cuk converter and the control design that mitigates the large disturbances in buck and boost modes have not been introduced in the literature.

This research aims to develop an averaged nonlinear model and design a current-mode controller for a bridgeless single-switch non-inverting ac-dc Cuk converter in DCM. The proposed controller is designed to track the desired output voltage during large line and load disturbances in buck and boost operation modes. The control system is developed to provide consistent dynamical response and maintain high power factor with low THD. MATLAB simulations are conducted to validate the proposed control scheme. The proposed controller is compared with the conventional PI controller to investigate the tracking performance of the two controllers under various operating conditions.

II. Modeling of Bridgeless AC-DC Cuk Converter

The circuit of the bridgeless single-switch non-inverting ac-dc Cuk PFC converter is shown in Fig. 1(a). The principle of operation, the steady-state analysis, and the converter design have been introduced in [3]. The polarities of the switch S_1 and diodes D_P, D_N, D_o, D_1, and D_2 are arranged such that the current flow yields a positive output voltage.

Since the operation is symmetrical in two half-line cycles of input voltage, the power converter model is developed during one switching period in the positive half-line cycle. In DCM, the ac-dc Cuk converter exhibits three configurations during the switching period. As shown in Fig. 1(b), when S_1 is

ON and D_o is OFF, the system dynamics can be derived using Kirchhoff's voltage and current laws, yielding

$$\begin{cases} \frac{di_{L_2}}{dt} = \frac{v_I}{L_2} \\ \frac{di_{L_o}}{dt} = -\frac{v_{C_2}}{L_o} - \frac{v_{C_o}}{L_o} \\ \frac{dv_{C_2}}{dt} = \frac{i_{L_o}}{C_2} \\ \frac{dv_{C_o}}{dt} = \frac{i_{L_o}}{C_o} - \frac{v_{C_o}}{RC_o}. \end{cases} \tag{1}$$

Fig. 1(c) shows the ac-dc converter circuit when S_1 is OFF and D_o is ON. Kirchhoff's voltage and current laws give

$$\begin{cases} \frac{di_{L_2}}{dt} = -\frac{v_{C_2}}{L_2} + \frac{v_I}{L_2} \\ \frac{di_{L_o}}{dt} = -\frac{v_{C_o}}{L_o} \\ \frac{dv_{C_2}}{dt} = \frac{i_{L_2}}{C_2} \\ \frac{dv_{C_o}}{dt} = \frac{i_{L_o}}{C_o} - \frac{v_{C_o}}{RC_o}. \end{cases} \tag{2}$$

Finally, when both S_1 and D_o are OFF as in Fig. 1(d), one gets

$$\begin{cases} \frac{di_{L_2}}{dt} = -\frac{v_{C_2}}{L_o+L_2} - \frac{v_{C_o}}{L_o+L_2} + \frac{v_I}{L_o+L_2} \\ \frac{di_{L_o}}{dt} = -\frac{v_{C_2}}{L_o+L_2} - \frac{v_{C_o}}{L_o+L_2} + \frac{v_I}{L_o+L_2} \\ \frac{dv_{C_2}}{dt} = \frac{i_{L_2}}{C_2} \\ \frac{dv_{C_o}}{dt} = \frac{i_{L_o}}{C_o} - \frac{v_{C_o}}{RC_o}. \end{cases} \tag{3}$$

During the third time interval defined by (3), L_o and L_2 act as constant current source [3]. It should be noted that the inductors current in (3) requires correction to apply the averaging theory [14]. Thus, the averaged inductors current during the switching period T can be described as follows

$$\begin{cases} \bar{i}_{L_2} = \frac{1}{T}\int_0^T i_{L_2} dt = i_x + \frac{(d_1+d_2)(d_1 T)v_I}{2L_2} \\ \bar{i}_{L_o} = \frac{1}{T}\int_0^T i_{L_o} dt = i_x - \frac{(d_1+d_2)(d_1 T)(v_{C_2}+v_{C_o})}{2L_o}, \end{cases} \tag{4}$$

where d_1 and d_2 are the first- and second-time intervals, respectively. Using (4), the current i_x is

$$i_x = \begin{cases} \bar{i}_{L_2} - \frac{(d_1+d_2)(d_1 T)v_I}{2L_2} \\ \bar{i}_{L_o} + \frac{(d_1+d_2)(d_1 T)(v_{C_2}+v_{C_o})}{2L_o}. \end{cases} \tag{5}$$

Hence, subtracting $\bar{i}_{L_o}$ from $\bar{i}_{L_2}$ gives d_2, which is

$$d_2 = \frac{2\left(\bar{i}_{L_2} - \bar{i}_{L_o}\right)}{d_1 T\left(\frac{v_I}{L_2} + \frac{v_{C_2}+v_{C_o}}{L_o}\right)} - d_1. \tag{6}$$

Using the averaging technique [15], [16], the averaged nonlinear model of the Cuk PFC converter can be expressed as

$$\begin{cases} \frac{d\bar{i}_{L_2}}{dt} = \frac{\bar{v}_I}{L_2} d_1 + \frac{\bar{v}_I - \bar{v}_{C_2}}{L_2} d_2 + \frac{\bar{v}_I - \bar{v}_{C_2} - \bar{v}_{C_o}}{L_o+L_2}(1 - d_1 - d_2) \\ \frac{d\bar{i}_{L_o}}{dt} = -\frac{\bar{v}_{C_2}+\bar{v}_{C_o}}{L_o} d_1 - \frac{\bar{v}_{C_o}}{L_o} d_2 + \frac{\bar{v}_I - \bar{v}_{C_2} - \bar{v}_{C_o}}{L_o+L_2}(1 - d_1 - d_2) \\ \frac{d\bar{v}_{C_2}}{dt} = \frac{\bar{i}_{L_o}}{C_2} d_1 + \frac{\bar{i}_{L_2}}{C_2} d_2 + \frac{i_x}{C_2}(1 - d_1 - d_2) \\ \frac{d\bar{v}_{C_o}}{dt} = \frac{\bar{i}_{L_o}}{C_o} - \frac{\bar{v}_{C_o}}{RC_o}. \end{cases} \tag{7}$$

The steady-state waveforms of V_{GS}, I_{L_2}, and I_{L_o} of the simulated bridgeless Cuk converter model are shown in Fig. 2.

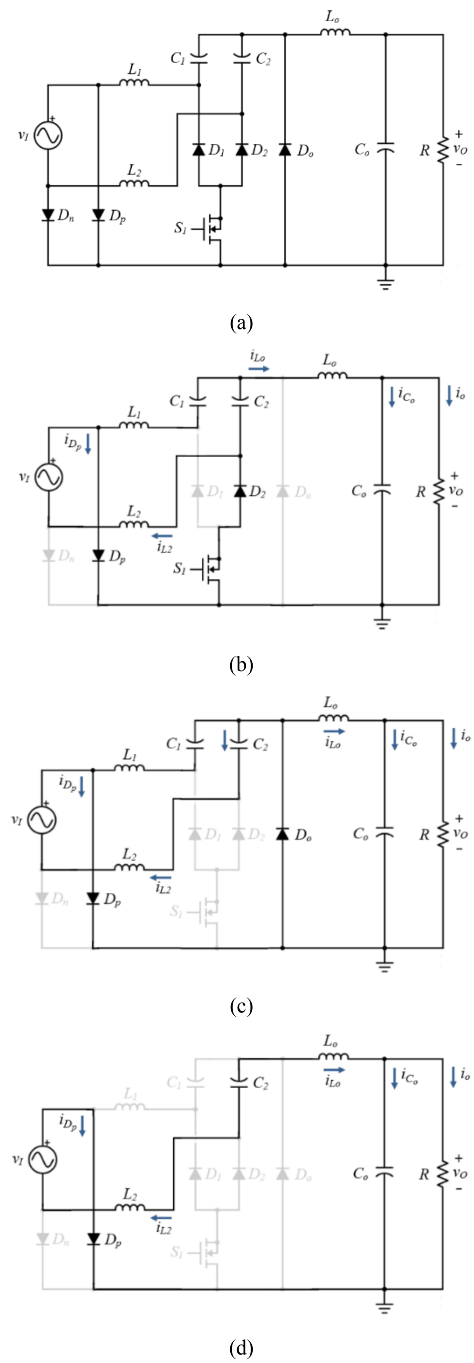

Fig. 1. The ac-dc Cuk PFC converter. (a) The circuit. The circuit when (b) S_1 is ON and D_o is OFF, (c) S_1 is OFF and D_o is ON, and (d) S_1 and D_o are OFF.

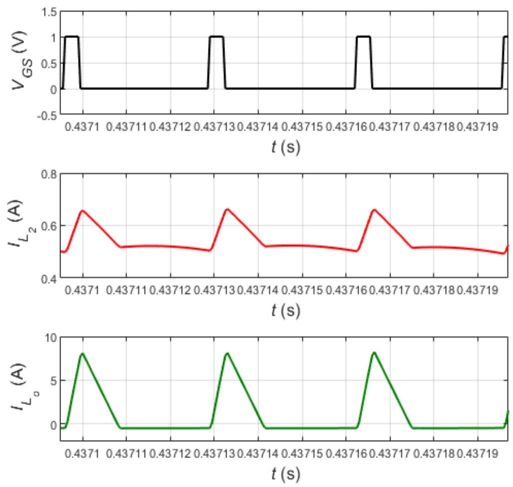

Fig. 2. The steady-state waveforms of the gate-to-source V_{GS}, input inductor current I_{L2}, and output inductor current I_{Lo} of the ac-dc Cuk converter model.

III. Current-Mode Control Law

As depicted in Fig. 3, the current-mode control scheme consists of two loops. The outer voltage loop contains the voltage error signal, which passes through a proportional-integral compensator. The inner current loop, on the other hand, contains the rectified input inductor current signal, which is scaled by a constant gain (K). Like the sliding-mode current control method [17], [18], the outer loop creates a reference current signal i_R that is given by

$$i_R = K_p(V_r - \beta v_o) + K_I \int (V_r - \beta v_o)dt. \tag{8}$$

The reference current contains the integral term of the output voltage error, which eliminates the steady-state error. The measured inductor current i_{L_2} tracks the reference current profile i_R to generate a control signal u that can be expressed as

$$u = K_p(V_r - \beta v_o) + K_I \int (V_r - \beta v_o)dt - K|i_{L_2}|. \tag{9}$$

Next, the PWM generator compares the control signal u with a saw tooth waveform to generate the duty cycle that tracks the desired inductor current and regulates the output voltage.

TABLE I. Parameters of AC-DC Cuk PFC Converter

Description	Parameter	Value
Input Inductance	L_1, L_2	2.5 mH
Output Inductance	L_o	47 μH
Input Capacitance	C_1, C_2	1 μF
Output Capacitance	C_o	3.3 mF
Nominal Load Resistance	R	80 Ω
Input Voltage	v_I	(80 - 160) VAC
Input Frequency	f	60 Hz
Output Voltage	v_O	(48 - 220) VDC
Switching Frequency	f_s	30 kHz

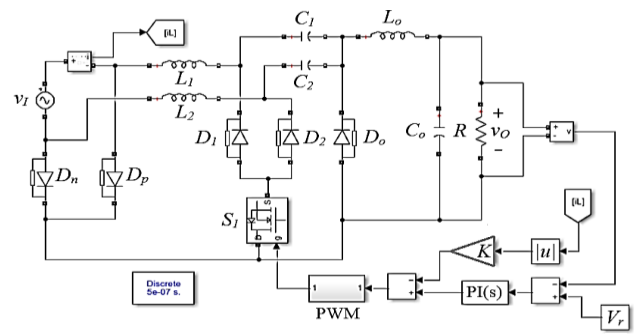

Fig. 3. MATLAB/SIMULINK model of the proposed current-mode controlled bridgeless single-switch non-inverting ac-dc Cuk converter.

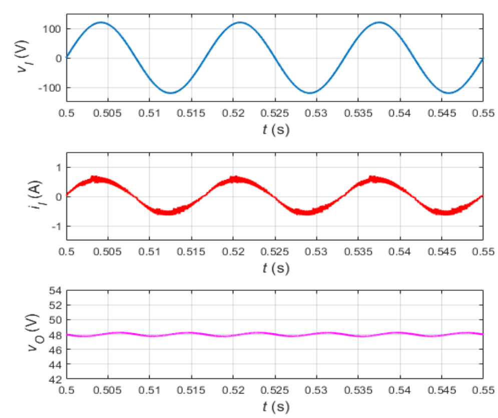

(a)

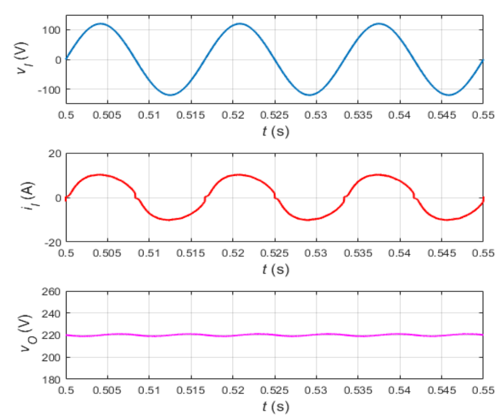

(b)

Fig. 4. The steady-state waveforms of the input voltage v_I, input current i_I, and output voltage v_O during (a) buck and (b) boost modes.

IV. Results and Discussion

A. Steady-State Performance

Ziegler–Nichols method is utilized to design the controller gains based on the ac-dc converter model. The converter parameters are given in Table I, which are selected according to [2]. The controller gains K, K_p, and K_I are set to 0.02, 0.015, and 1.45, respectively. The steady-state waveforms of v_I, i_I, and

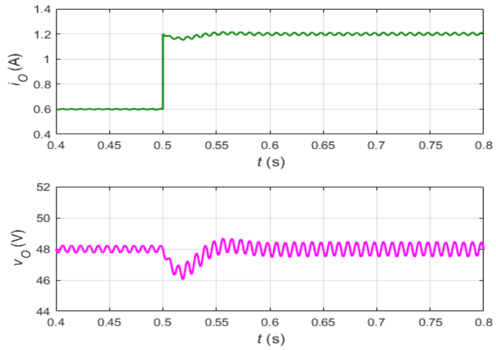

(a)

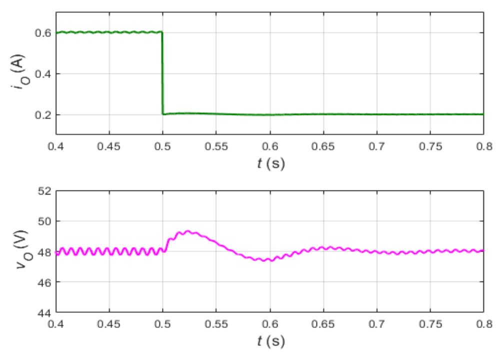

(b)

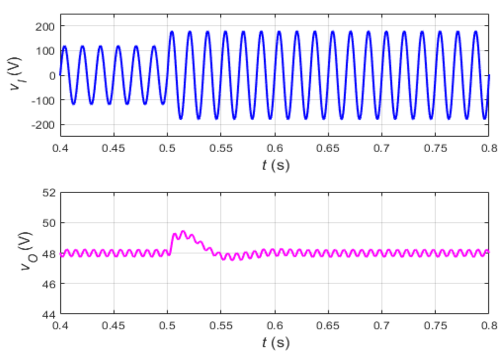

(c)

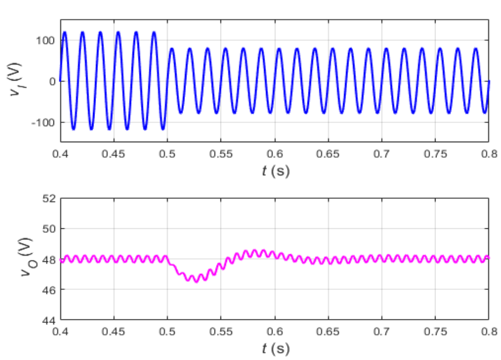

(d)

Fig. 5. The tracking performance of the proposed controller in buck mode during abrupt change in (a) - (b) load current and (c) - (d) input voltage.

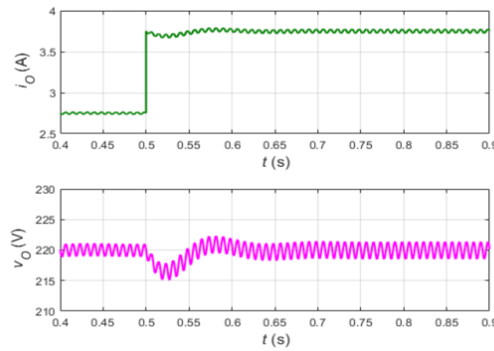

(a)

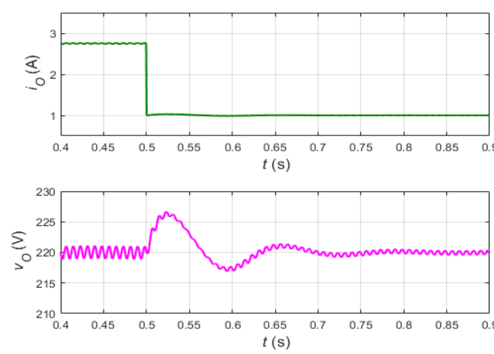

(b)

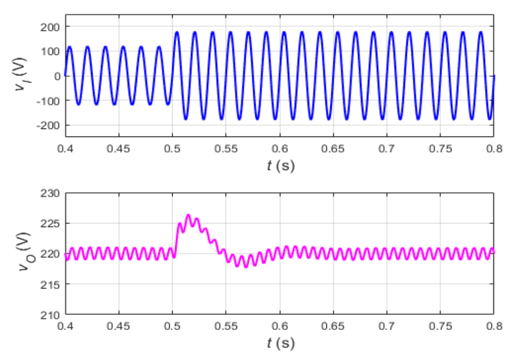

(c)

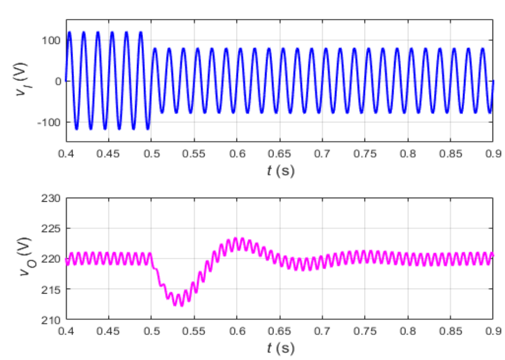

(d)

Fig. 6. The tracking performance of the proposed controller in boost mode during abrupt change in (a) - (b) load current and (c) - (d) input voltage.

TABLE II. TRANSIENT RESPONSE CHARACTERISTICS OF CURRENT-MODE CONTROLLED BRIDGELESS AC-DC CUK CONVERTER

Operation Mode	**Line/Load Disturbance**	***PO/PU* (%)**	**t_s (ms)**	**V_O (V)**
Buck	$V_I = 120 \rightarrow 80.0$ (V)	3.1	100	48
	$V_I = 120 \rightarrow 180$ (V)	3.1	50	
	$I_O = 0.6 \rightarrow 1.2$ (A)	4.0	40	
	$I_O = 0.6 \rightarrow 0.2$ (A)	2.8	125	
Boost	$V_I = 120 \rightarrow 80.0$ (V)	3.6	150	220
	$V_I = 120 \rightarrow 180$ (V)	2.9	100	
	$I_O = 2.75 \rightarrow 3.75$ (A)	2.2	50	
	$I_O = 2.75 \rightarrow 1.00$ (A)	3	175	

v_O during buck and boost modes are shown in Fig. 4(a) and (b), respectively. It has been noticed that at R = 80 Ω, the control scheme converts 120 VAC input to 48/220 VDC output, while the power factor is about 0.99. The THD in the buck and boost modes is 8.2 % and 10.4 %, respectively.

B. Tracking Performance during Line and Load Disturbances

The tracking performance of the closed-loop converter during abrupt changes in line voltage and load current is analyzed in buck and boost modes. Table II summaries the transient response characteristics during these disturbances.

During the buck operation mode, Fig. 5(a) and (b) shows the system response when the load current i_O changes from 0.6 A to 1.2 A and from 0.6 A to 0.2 A, respectively. On the other hand, Fig. 5(c) and (d) shows the response when the input voltage v_I changes from 120 VAC to 180 VAC and from 120 VAC to 80 VAC, respectively. Table II shows that the maximum percentage undershoot *PU* is 4 % when i_O changes from 0.6 A to 1.2 A. Moreover, the longest settling time t_s is about 125 ms when i_O changes from 0.6 A to 0.2 A.

Fig. 6(a) - (d) shows the response during the load and line disturbances while the converter is operating in boost mode. As shown in Table II, the maximum *PU* is 3.6 % when v_I changes from 120 VAC to 80 VAC. On the other hand, the longest t_s is about 175 ms when i_O changes from 2.75 A to 1.0 A. Hence, the current-mode controlled ac-dc Cuk converter tracks the desired output voltage in the presence of line and load disturbances. In addition, the transient response characteristics are maintained within 4 % percentage overshoot/undershoot and 175 ms settling time.

C. Comparison with Voltage-Mode Controller

Fig. 7 and 8 exhibit the tracking performance of the proposed current-mode and the classical PI control schemes under line and load disturbances. The parameters K_p and K_I are

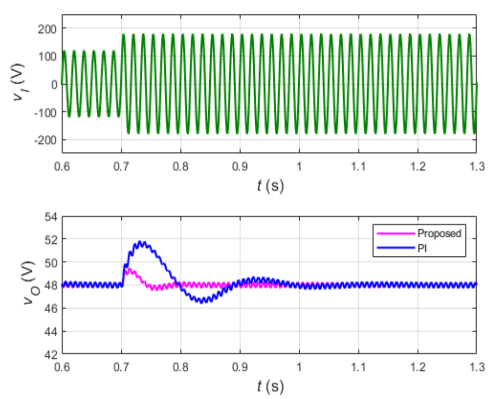

(a)

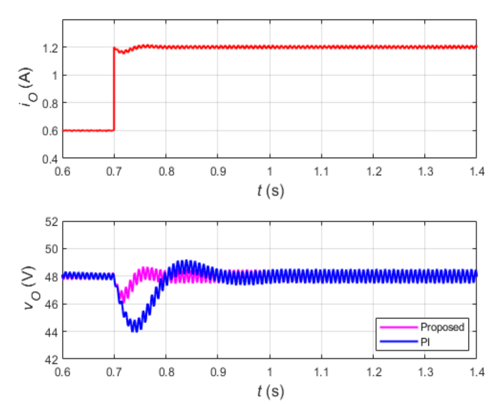

(b)

Fig. 7. The tracking performance of the proposed current-mode and classical PI controllers during (a) line and (b) load disturbances in buck mode.

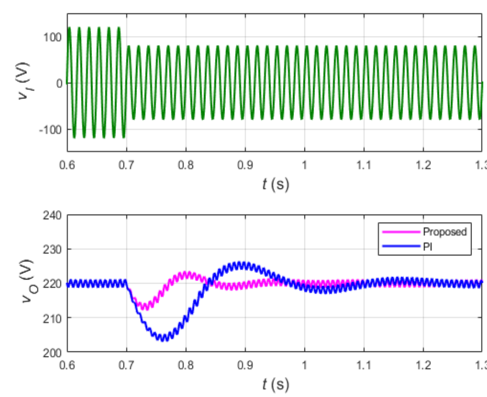

(a)

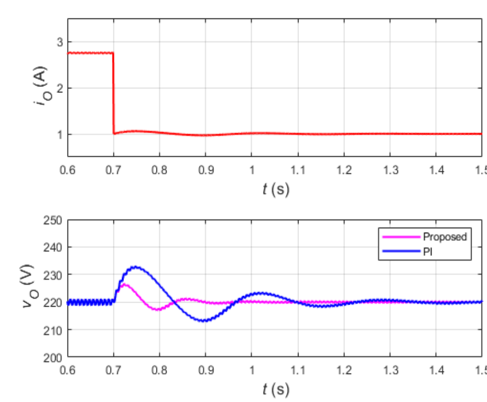

(b)

Fig. 8. The tracking performance of the proposed current-mode and classical PI controllers during (a) line and (b) load disturbances in boost mode.

TABLE III. COMPARISON OF PROPOSED AND PI CONTROL PERFORMANCE

Operation Mode	Controller	Line/Load Disturbance	*PO/PU* (%)	t_s (ms)
Buck	Proposed	$V_I = 120 \rightarrow 180$ (V)	3.1	50
	PI		7.9	300
	Proposed	$I_O = 0.6 \rightarrow 1.2$ (A)	4.0	40
	PI		8.3	175
Boost	Proposed	$V_I = 120 \rightarrow 80.0$ (V)	3.6	150
	PI		7.7	400
	Proposed	$I_O = 2.75 \rightarrow 1.00$ (A)	3	175
	PI		5.9	500

selected using Ziegler–Nichols method to operate the bridgeless ac-dc Cuk converter model in buck and boost modes. Thus, the gains of the classical PI controller K_p and K_I are set to 0.003 and 0.22, respectively. The proposed current-mode controller u and the classical PI controller u^* are given as

$$\begin{cases} u = 0.015(V_r - \beta v_o) + 1.45 \int (V_r - \beta v_o)dt - 0.02|i_{L_2}| \\ u^* = 0.003(V_r - \beta v_o) + 0.22 \int (V_r - \beta v_o)dt. \end{cases} \quad (10)$$

The two closed-loop control schemes of the bridgeless non-inverting power converter in DCM are simulated in MATLAB/SIMULINK. The transient response characteristics of the control schemes are summarized in Table III.

It can be seen that the proposed controller response exhibits lower percentage overshoot/undershoot *PO/PU* and shorter settling time t_s as compared to those of the PI controller. Notably, the absence of the inductor current component i_{L_2} in the classical voltage-mode controller u^* results in a slow dynamical response with a limited bandwidth due to the non-minimum phase property of the power converter. In contrast, the proposed controller u tracks the reference current signal, accommodates the non-minimum phase property, regulates the output voltage, and improves the dynamical response of the closed-loop power converter.

V. CONCLUSION

The averaged nonlinear model of the bridgeless single-switch non-inverting ac-dc Cuk converter in DCM has been derived. Additionally, a current-mode control scheme has been designed to provide regulated dc output voltage higher or lower than the ac input voltage. It has been confirmed that the proposed control scheme tracks the desired output voltage in the presence of the line and load disturbances and maintains consistent dynamical response. The comparison with the PI controller has shown the superiority of the proposed controller, where the latter exhibits faster transient response with lower percentage overshoot. Further, due to the non-inverting single-switch ac-dc Cuk converter typology, the proposed current-mode control scheme has become simpler than those with a negative output voltage and multiple switches.

REFERENCES

[1] A. Reatti, F. Corti, A. Tesi, A. Torlai and M. K. Kazimierczuk, “Nonlinear exact analysis and solution of power stage of DC-DC PWM boost converter,” *2019 IEEE International Symposium on Circuits and Systems (ISCAS)*, 2019, pp. 1-5.

[2] Z. Zhang *et al.*, “Analysis and design of a single-stage bridgeless isolated AC-DC resonant converter for programmable AC power source applications,” in *IEEE Access*, vol. 8, pp. 219071-219082, 2020.

[3] H. Yang, H. Chiang and C. Chen, “Implementation of bridgeless Cuk power factor corrector with positive output voltage,” in *IEEE Transactions on Industry Applications*, vol. 51, no. 4, pp. 3325-3333, July-Aug. 2015.

[4] G. Li, J. Xia, K. Wang, Y. Deng, X. He and Y. Wang, “A single-stage interleaved resonant bridgeless boost rectifier with high-frequency isolation,” in *IEEE Journal of Emerging and Selected Topics in Power Electronics*, vol. 8, no. 2, pp. 1767-1781, June 2020.

[5] H. Valipour, M. Mahdavi and M. Ordonez, “Resonant bridgeless AC/DC rectifier with high switching frequency and inherent PFC capability,” in *IEEE Transactions on Power Electronics*, vol. 35, no. 1, pp. 232-246, Jan. 2020.

[6] Y. Liu, X. Huang, Y. Dou, Z. Ouyang and M. A. E. Andersen, “GaN-based ZVS bridgeless dual-SEPIC PFC rectifier with integrated inductors,” in *IEEE Transactions on Power Electronics*, vol. 36, no. 10, pp. 11483-11498, Oct. 2021.

[7] K. K. M. Siu and C. N. M. Ho, “Manitoba rectifier—bridgeless buck–boost PFC,” in *IEEE Transactions on Power Electronics*, vol. 35, no. 1, pp. 403-414, Jan. 2020.

[8] N. Molavi, M. Maghsoudi and H. Farzanehfard, “Quasi-resonant bridgeless PFC converter with low input current THD,” in *IEEE Transactions on Power Electronics*, vol. 36, no. 7, pp. 7965-7972, July 2021.

[9] H. Wu, Y. Zhang and Y. Jia, “Three-port bridgeless PFC-based quasi single-stage single-phase AC–DC converters for wide voltage range applications,” in *IEEE Transactions on Industrial Electronics*, vol. 65, no. 7, pp. 5518-5528, July 2018.

[10] Y. Jeong, M. Park and G. Moon, “High-efficiency zero-voltage-switching totem-pole bridgeless rectifier with integrated inrush current limiter circuit,” in *IEEE Transactions on Industrial Electronics*, vol. 67, no. 9, pp. 7421-7429, Sept. 2020.

[11] J. W. -T. Fan, R. S. -C. Yeung and H. S. -H. Chung, “Optimized hybrid PWM scheme for mitigating zero-crossing distortion in totem-pole bridgeless PFC,” in *IEEE Transactions on Power Electronics*, vol. 34, no. 1, pp. 928-942, Jan. 2019.

[12] V. Bist and B. Singh, “A unity power factor bridgeless isolated Cuk converter-fed brushless DC motor drive,” in *IEEE Transactions on Industrial Electronics*, vol. 62, no. 7, pp. 4118-4129, July 2015.

[13] M. Mahdavi and H. Farzaneh-Fard, “Bridgeless Cuk power factor correction rectifier with reduced conduction losses,” *IET Power Electronics*, vol. 5, no. 9, pp. 1733-1740, Sept. 2012.

[14] E. Arango, C. A. Ramos-Paja, R. Giral, S. Serna and G. Petrone, “Modeling and control of Cuk converter operating in DCM” in *Electrical Engineering and Control*, Berlin, Germany: Springer, vol. 98, pp. 441-449, 2011.

[15] H. Al-Baidhani, M. K. Kazimierczuk and A. Reatti, “Nonlinear modeling and voltage-mode control of DC-DC boost converter for CCM,” *2018 IEEE International Symposium on Circuits and Systems (ISCAS)*, 2018, pp. 1-5.

[16] A. Reatti, F. Corti, A. Tesi, A. Torlai and M. K. Kazimierczuk, “Effect of parasitic components on dynamic performance of power stages of DC-DC PWM buck and boost converters in CCM,” *2019 IEEE International Symposium on Circuits and Systems (ISCAS)*, 2019, pp. 1-5.

[17] H. Al-Baidhani and M. K. Kazimierczuk, “PWM-based proportional-integral sliding-mode current control of DC-DC boost converter,” *2018 IEEE Texas Power and Energy Conference (TPEC)*, 2018, pp. 1-6.

[18] H. Al-Baidhani, M. K. Kazimierczuk and R. Ordóñez, “Nonlinear modelling and control of PWM DC-DC buck-boost converter for CCM,” *IECON 2018 - 44th Annual Conference of the IEEE Industrial Electronics Society*, 2018, pp. 1374-1379.